

Local background estimation and the replacement target model

James Theiler and Amanda Ziemann

Los Alamos National Laboratory, Los Alamos, NM 87545

ABSTRACT

We investigate the detection of opaque targets in cluttered multi/hyper-spectral imagery, using a local background estimation model. Unlike transparent “additive-model” targets (like gas-phase plumes), these are solid “replacement-model” targets, which means that the observed spectrum is a linear combination of the target signature and the background signature. Pixels with stronger targets are associated with correspondingly weaker backgrounds, and background estimators can over-estimate the background in a target pixel. In particular, “subtracting the background” (which generalizes the usual notion of subtracting the mean) to produce a residual image can actually have deleterious effect. We examine an adaptive partial background subtraction scheme, and evaluate its utility for the detection of replacement-model targets.

Keywords: hyperspectral imagery, target detection, background estimation, residual

1. INTRODUCTION

To detect weak or rare signals in a cluttered background, a key first step is to model that background.¹ The classic choice – seemingly naive, but popular, and often quite effective – is a simple multivariate Gaussian distribution, with a single global mean and a single global covariance. Both additive target detectors (such as adaptive matched filter²⁻⁴ [AMF], the adaptive coherence estimator^{5,6} [ACE], or the hybrid elliptically-contoured generalized likelihood ratio test⁷ [EC-GLRT]), and replacement target detectors (such as mixture-tuned matched filter⁸ [MTMF], matched filter with false alarm mitigation⁹ [MF-FAM], or finite target matched filter¹⁰ [FTMF]), have been developed for the global Gaussian background, though the additive models are more commonly used. In part this is because they are easier to compute, but also because they often provide reasonable target detection performance even for targets that are more physically well-represented by the replacement model.

A potentially more accurate model of the background at a given pixel is to compute a local mean, based on an annulus surrounding that pixel.¹¹⁻¹⁵ This is effectively a high-pass filter, and is related to the “unsharp mask” approach^{16,17} for detecting point targets. Further accuracy can be obtained by considering the background pixel value to be an arbitrary function of the annulus pixels, and then fitting a regression of the center pixel as a function of the annulus pixels.¹⁸⁻²⁰

Subtracting the estimated background from the observed image yields a “residual” image that can be used for target detection. See Fig. 2 for an illustration of the residual image. With a better estimate of the background, one might presume that target detection performance would be improved. This was not observed in work reported previously,²¹ and in that work, we speculated that the culprit might be the fact that the target signal is not strictly additive.²² To test that hypothesis, we develop an adaptive residual that respects a replacement model, instead of an additive model, for targets in a scene.

Email: jt@lanl.gov, ziemann@lanl.gov

Table 1. Notation

d	Number of spectral channels in hyperspectral image
$\mathbf{y} \in \mathbb{R}^d$	Pixel under test
$\mathbf{t} \in \mathbb{R}^d$	Target signature
$\alpha \in \mathbb{R}$	Strength, size, or quantity of target
$\tilde{\mathbf{y}} \in \mathbb{R}^d$	Background spectrum at pixel under test
$\mathbf{x} \in \mathbb{R}^d$	Pixel in the annulus surrounding center pixel \mathbf{y}
$\mathbf{X} \in \mathbb{R}^{kd}$	Concatenation of k pixels in the annulus surrounding center pixel
$f : \mathbb{R}^{kd} \rightarrow \mathbb{R}^d$	Function estimating pixel \mathbf{y} based on the annulus pixels \mathbf{X}
$\hat{\mathbf{y}} \in \mathbb{R}^d$	Estimate of \mathbf{y} , given by $\hat{\mathbf{y}} = f(\mathbf{X})$

2. WHAT'S WRONG WITH RESIDUALS?

LGOP: Looked good on paper
— *Acronym Dictionary*
(as related by David Messinger)

Let \mathbf{y} be a pixel of interest, which may or may not include target signature. Let $\tilde{\mathbf{y}}$ be the “background” at that pixel. It is (if this makes sense) what the pixel spectrum *would have been* if there were no target present in the pixel. (For pixels in which a target is not actually present, which is usually the vast majority of pixels in an image, $\tilde{\mathbf{y}} = \mathbf{y}$.) In terms of $\tilde{\mathbf{y}}$, we can employ either an additive model

$$\mathbf{y} = \tilde{\mathbf{y}} + \alpha \mathbf{t}, \quad (1)$$

or a replacement model

$$\mathbf{y} = (1 - \alpha)\tilde{\mathbf{y}} + \alpha \mathbf{t}, \quad (2)$$

to describe the pixel of interest \mathbf{y} in terms of a background $\tilde{\mathbf{y}}$ and a known target signature \mathbf{t} . Here, the scalar value α corresponds to some measure of the “strength” of the target signal in that pixel. For the replacement model, α is often interpreted as the areal size of the target compared to the size of the pixel. For a pixel that is pure background, we would have $\alpha = 0$; and for a pixel that is pure target, $\alpha = 1$.

Using the regression framework,¹⁸ we can estimate \mathbf{y} with a function of the pixels $\mathbf{X} = [\mathbf{x}_1, \mathbf{x}_2, \dots]$ surrounding \mathbf{y} : that is (see Fig. 1),

$$\hat{\mathbf{y}} = f(\mathbf{X}). \quad (3)$$

But what $\hat{\mathbf{y}}$ is approximating is not really \mathbf{y} , but that phantom $\tilde{\mathbf{y}}$. That’s because the surrounding pixels \mathbf{X} don’t “know” whether or not there is a target in \mathbf{y} . Eq. (3) describes a very general scenario, but it includes, in the simplest case, the estimate of \mathbf{y} with a global mean; *i.e.*, $\hat{\mathbf{y}} = \boldsymbol{\mu}$, where $\boldsymbol{\mu}$ is the mean of all the pixel values \mathbf{y} in the image. We remark that this kind of global mean subtraction is a standard protocol in hyperspectral target detection.

A simple residual image is given by

$$\mathbf{e} = \mathbf{y} - \hat{\mathbf{y}} = \mathbf{y} - f(\mathbf{X}) \quad (4)$$

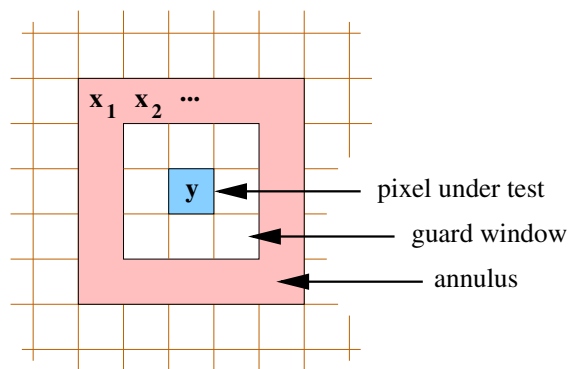


Figure 1. The center pixel \mathbf{y} is estimated as a function of the pixels $\mathbf{X} = [\mathbf{x}_1, \mathbf{x}_2, \dots]$ in an annulus surrounding the center pixel (and, possibly, a guard window, to reduce the contamination of the background estimate by a target that may not be entirely contained in the center pixel). The estimator $\hat{\mathbf{y}} = f(\mathbf{X})$ could be a simple mean of the pixels \mathbf{X} in the annulus, or a more complicated function.

and if we are looking for target in the pixel \mathbf{y} , we can apply our favorite detector to this residual. For instance, writing $E = \langle \mathbf{e}\mathbf{e}^T \rangle$ as the covariance matrix of the residuals, the ACE detector is given by

$$\mathcal{D}(\mathbf{e}) = \frac{\mathbf{t}^T E^{-1} \mathbf{e}}{\sqrt{\mathbf{t}^T E^{-1} \mathbf{t}} \sqrt{\mathbf{e}^T E^{-1} \mathbf{e}}} = \cos_E(\mathbf{t}, \mathbf{e}) \quad (5)$$

where we write $\cos_A(\mathbf{b}, \mathbf{c})$ to be the cosine of the angle between the vectors $A^{-1/2}\mathbf{b}$ and $A^{-1/2}\mathbf{c}$; as such, it is bounded between -1 and $+1$. Further, for any positive scalars p and q , we have that $\cos_A(p\mathbf{b}, q\mathbf{c}) = \cos_A(\mathbf{b}, \mathbf{c})$.

To the extent that $\hat{\mathbf{y}}$ is a good approximation for $\tilde{\mathbf{y}}$, we can write $\mathbf{e} \approx \mathbf{y} - \tilde{\mathbf{y}}$. And for the additive model, we can invoke Eq. (1) to write $\mathbf{e} \approx \alpha\mathbf{t}$; thus, $\mathcal{D}(\mathbf{e}) \approx \cos_E(\mathbf{t}, \alpha\mathbf{t}) = \cos_E(\mathbf{t}, \mathbf{t}) = 1$ approaches its maximum value. This suggests that residuals can be effectively combined with the ACE detector to find additive targets in imagery.

Actually, this ‘ \approx ’ argument is pretty informal. An only slightly more formal argument writes $\mathbf{e} = \alpha\mathbf{t} + (\tilde{\mathbf{y}} - \hat{\mathbf{y}})$. Thus, $\mathcal{D}(\mathbf{e}) = \cos_E(\mathbf{t}, \alpha\mathbf{t} + (\tilde{\mathbf{y}} - \hat{\mathbf{y}})) = \cos_E(\mathbf{t}, \mathbf{t} + (\tilde{\mathbf{y}} - \hat{\mathbf{y}})/\alpha)$, which illustrates that fact that as α becomes small, the mismatch between $\tilde{\mathbf{y}}$ and $\hat{\mathbf{y}}$ becomes more important. To say this another way: the weaker the target, the better the background model needs to be.

Now consider the replacement model. Here, the residual, as given by Eq. (4), is approximated by $\mathbf{e} = \mathbf{y} - \hat{\mathbf{y}} \approx \mathbf{y} - \tilde{\mathbf{y}} = (1 - \alpha)\tilde{\mathbf{y}} + \alpha\mathbf{t} - \tilde{\mathbf{y}} = \alpha(\mathbf{t} - \tilde{\mathbf{y}})$. And thus,

$$\mathcal{D}(\mathbf{e}) = \cos_E(\mathbf{t}, \mathbf{e}) = \cos_E(\mathbf{t}, \mathbf{t} - \tilde{\mathbf{y}}) \quad (6)$$

and we see that to the extent \mathbf{t} and $\tilde{\mathbf{y}}$ are not parallel, $\mathcal{D}(\mathbf{e})$ will be bounded away from 1, even for relatively large values of α .

2.1 Adaptive residual

Consider a more general residual, in which we only subtract off part of the estimated background:

$$\mathbf{e} = \mathbf{y} - \beta\hat{\mathbf{y}} = \mathbf{y} - \beta f(\mathbf{X}) \quad (7)$$

and observe in this case that $\mathbf{e} = \alpha\mathbf{t} + (1 - \alpha)\tilde{\mathbf{y}} - \beta\hat{\mathbf{y}}$. If (perhaps being clairvoyant^{24–26}) we knew what α was ahead of time, we could use $\beta = 1 - \alpha$, and achieve

$$\mathcal{D}(\mathbf{e}) = \cos_E(\mathbf{t}, \mathbf{e}) = \cos_E(\mathbf{t}, \alpha\mathbf{t} + (1 - \alpha)(\tilde{\mathbf{y}} - \hat{\mathbf{y}})) \quad (8)$$

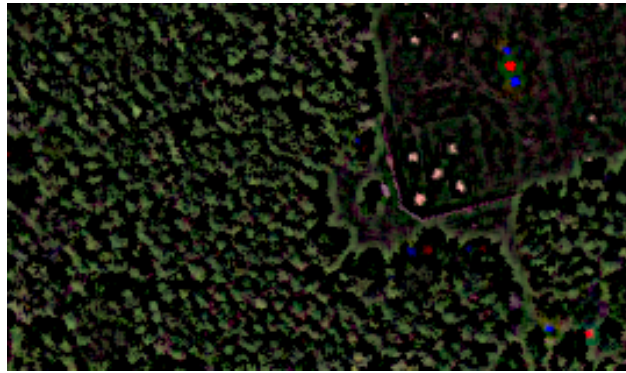
$$\approx \cos_E(\mathbf{t}, \alpha\mathbf{t}) = 1. \quad (9)$$



(a) Image \mathbf{y}



(b) Estimate $\hat{\mathbf{y}}$



(c) Residual $\mathbf{e} = \mathbf{y} - \hat{\mathbf{y}}$

Figure 2. Shown is a red-green-blue (RGB) image of (a) the initial SHARE 2012 hyperspectral data cube under consideration,²³ (b) the estimated background image obtained using the regression framework, and (c) the residual image obtained by subtracting the estimate from the original.

In the unlucky circumstance that we are not clairvoyant, we need some *a priori* guess for α . For example, we might know that there is a range of full pixels and subpixels in an image so we might just use $\beta = 0.5$ as a kind of heuristic halfway guess.

Note that β could vary from pixel to pixel. Suppose we have some way to compute an estimator $\hat{\alpha}$ for α . Then $\beta = 1 - \hat{\alpha}$ would lead to a residual map of the form

$$\mathbf{e} = \mathbf{y} - (1 - \hat{\alpha})f(\mathbf{X}). \quad (10)$$

One such estimator was described by Schaum and Stocker¹⁰ as part of the derivation of the Finite Target Matched Filter; it is based on a generalized likelihood ratio test (GLRT) estimator for α . Alternatively, we can employ multiplication by a vector quantity to produce scalar values. We posit a vector \mathbf{a} , and use it in a dot product with both sides of Eq. (2) for the replacement model:

$$\mathbf{a}^\top \mathbf{y} = \alpha \mathbf{a}^\top \mathbf{t} + (1 - \alpha) \mathbf{a}^\top \tilde{\mathbf{y}}, \quad (11)$$

implies

$$\alpha = \frac{\mathbf{a}^\top (\mathbf{y} - \tilde{\mathbf{y}})}{\mathbf{a}^\top (\mathbf{t} - \tilde{\mathbf{y}})}, \quad (12)$$

which suggests the estimator

$$\hat{\alpha} = \frac{\mathbf{a}^\top (\mathbf{y} - f(\mathbf{X}))}{\mathbf{a}^\top (\mathbf{t} - f(\mathbf{X}))}. \quad (13)$$

To keep the denominator away from zero, we can take $\mathbf{a} = \mathbf{t} - f(\mathbf{X})$ to obtain

$$\hat{\alpha} = \frac{(\mathbf{t} - f(\mathbf{X}))^\top (\mathbf{y} - f(\mathbf{X}))}{\|\mathbf{t} - f(\mathbf{X})\|^2}, \quad (14)$$

and then the new adaptive residual in Eq. (7) becomes:

$$\mathbf{e} = \mathbf{y} - (1 - \hat{\alpha})f(\mathbf{X}) = \mathbf{y} - \left[1 - \frac{(\mathbf{t} - f(\mathbf{X}))^\top (\mathbf{y} - f(\mathbf{X}))}{\|\mathbf{t} - f(\mathbf{X})\|^2} \right] f(\mathbf{X}). \quad (15)$$

Should we decide to constrain $0 \leq \hat{\alpha} \leq 1$ (note that Eq. (13) includes no such constraints), then we can achieve that with

$$\mathbf{e} = \mathbf{y} - \mathcal{H} \left(1 - \frac{(\mathbf{t} - f(\mathbf{X}))^\top (\mathbf{y} - f(\mathbf{X}))}{\|\mathbf{t} - f(\mathbf{X})\|^2} \right) f(\mathbf{X}), \quad (16)$$

where

$$\mathcal{H}(z) = \begin{cases} 0 & \text{if } z \leq 0 \\ z & \text{if } 0 \leq z \leq 1 \\ 1 & \text{if } 1 \leq z \end{cases} \quad (17)$$

We remark that this residual, unlike the full residual (as shown, for instance, in Fig. 2), depends on the target \mathbf{t} . But for pixels in which the measured pixel \mathbf{y} and the target signature \mathbf{t} are orthogonal, *vis-a-vis* the local centroid $\hat{\mathbf{y}} = f(\mathbf{X})$, then $(\mathbf{t} - f(\mathbf{X}))^\top (\mathbf{y} - f(\mathbf{X})) = 0$ and our adaptive residual in Eq. (16) becomes $\mathbf{e} = \mathbf{y} - f(\mathbf{X})$, the same as the full residual.

3. EXPERIMENT

Our experiments are conducted on a georectified 170×280 pixel image with 360 spectral channels ranging from the visible to the short-wave infrared (wavelength range: $0.4\mu\text{m}$ - $2.45\mu\text{m}$). The dataset was collected by the SpectTIR VS sensor as part of the Rochester Institute of Technology Digital Imaging and Remote Sensing Laboratory's SHARE 2012 campaign.²³ In our experiments, we eliminate lower quality channels (1-6,115-127,129-139,144-152,178-210,253-291,341-360) which leaves us with 229 spectral channels. The pixel size on the ground is approximately one meter, and square red and blue felt cotton panels of size two and three meters on a side were placed in the scene prior to acquisition.

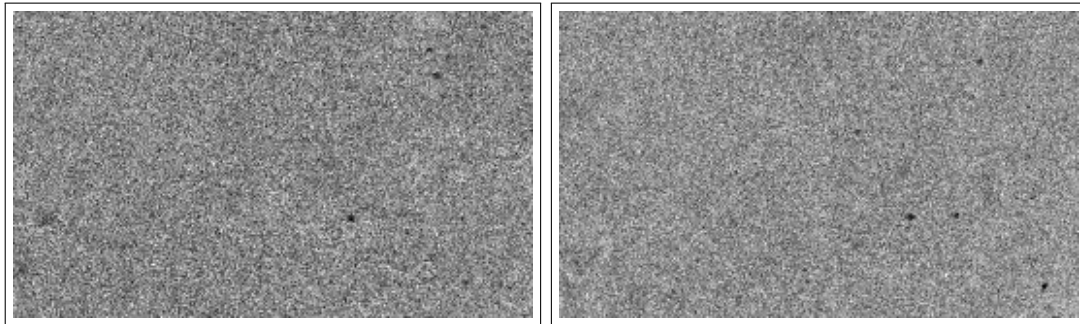
An RGB image of this data is shown in Fig. 2(a). At each pixel, a background level is estimated as a linear function of the pixels in a 13×13 annulus with a 5×5 guard window, and the resulting image is shown in Fig. 2(b). The estimated background image is, roughly speaking, a spatially smoothed version of the original image; because the smoothing kernel is the annulus, several ring-shaped artifacts are evident in the image. This is due to a kind of contamination of the background estimate with the target itself, but this contamination is not expected to be especially problematic.²⁷

In our first experiment, we try to detect the cotton felt panels using the ACE detector, with a laboratory-measured spectrum as the target signature. This is a reflectance spectrum, and to the extent that the image has been corrected for atmospheric and other effects, it should match the spectrum of the targets in the imagery. To the extent that these corrections are inexact, however, we expect some mismatch between the spectrum of the targets in the scene and the spectral signature that we use in our detection algorithm.

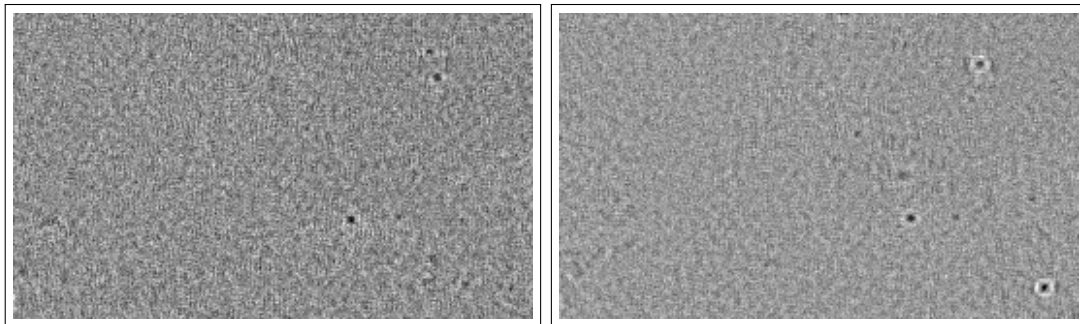
Fig. 3 shows the result of this first experiment, which uses only full residuals (assumes $\hat{\alpha} = 0$) using both local and global background estimation. In particular, the detection maps in Fig. 3(b,c)



(a) Truth Maps

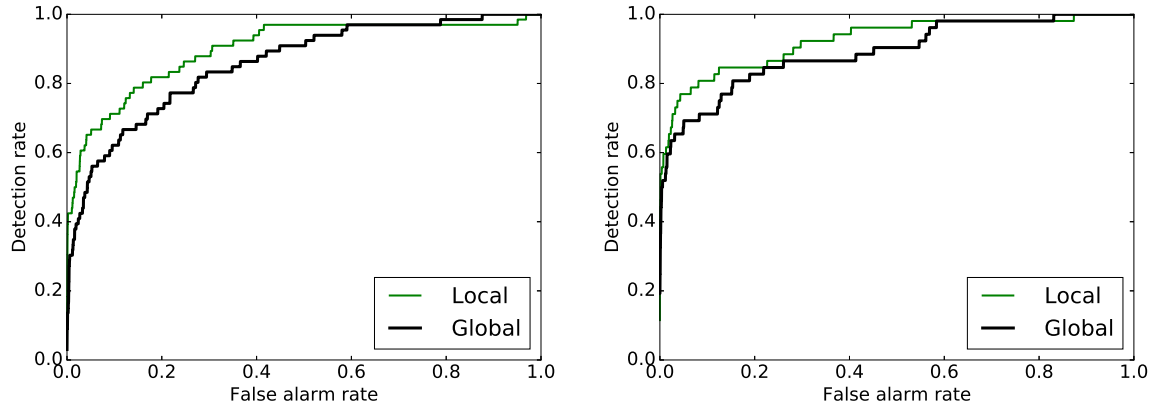


(b) Global Detection Maps



(c) Local Detection Maps

Figure 3. Left maps are for blue panel targets; right maps are for red panel targets. In these experiments the lab-measured target signatures are used for the blue and red panel targets.



(a) Blue panels

(b) Red panels

Figure 4. ROC curves compare target detection performance using locally and globally estimated backgrounds. In these experiments the lab-measured target signatures are used for (a) blue panels and (b) red panels.

are darker for pixels that are more likely to be targets. Both global and local detection maps are fairly unstructured, spatially, suggesting that the ACE detector is suppressing a lot of the background variability. The local maps appear to have slightly less variance, and they also exhibit a “halo”-like artifact around the detected targets (which is directly related to the ring-like artifacts observed in the local background estimate image). The ROC curves in Fig. 4 indicate the the local background estimators lead to better detection performance than the global background estimators, though the difference is not large, and the performance overall is anemic. (In this experiment, we saw virtually no difference between full versus adaptive residuals, so we only show the results with full residuals.)

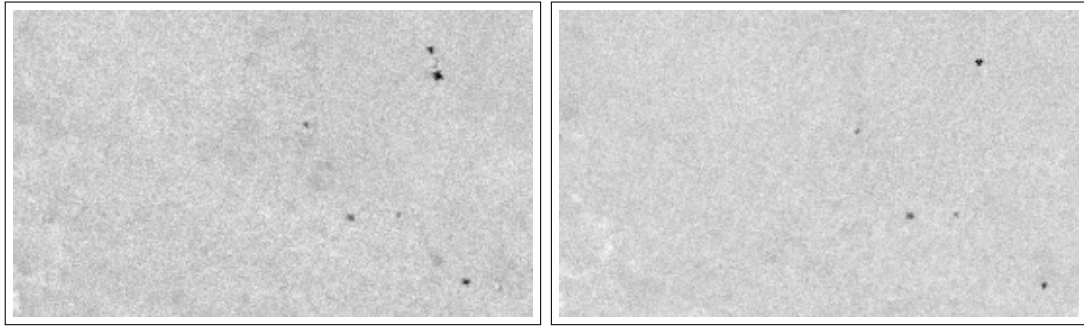
To improve the overall performance, we did a second experiment with a new target signature, this obtained by averaging all the in-scene target pixels. It is important to remark that this experiment is not operationally plausible – if you knew all the target pixels in the image, there’d be no need to do target detection. Nonetheless, this eliminates the confound of spectral mismatch, and concentrates on the effects of background subtraction. We expect (and indeed we see) much better performance overall.

In this experiment, comparing the global to local, using the full residual, we obtained the counter-intuitive result that the globally estimated background led to better detection than the more accurate locally estimated background. (This is the result we reported in last year’s SPIE paper²¹ and that inspired the current research.) We can begin to see this in the detection maps, in Fig. 5(a,b), and even more clearly in the ROC curves, in Fig. 6.

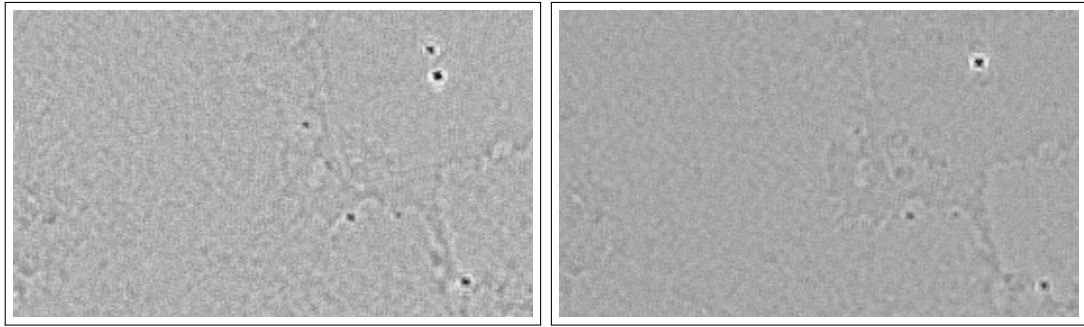
But when we use the adaptive residual, the results improve. For both the red and blue panels, the adaptive residual leads to better performance than the full residual. Fig. 5(c) shows the estimated $\hat{\alpha}$, which corresponds to (but does not exactly match) the detection maps, and Fig. 5(d) shows detection maps using the adaptive residuals. Comparing Fig. 5(b) and Fig. 5(d), we see that the detection map background has less evident spatial structure in the adaptive case. And more to the point, the ROC curves in Fig. 6 show better performance for the adaptive vs full residuals in all cases. Indeed, it bears remarking that the adaptive residual even improves the global background estimator.

4. DISCUSSION

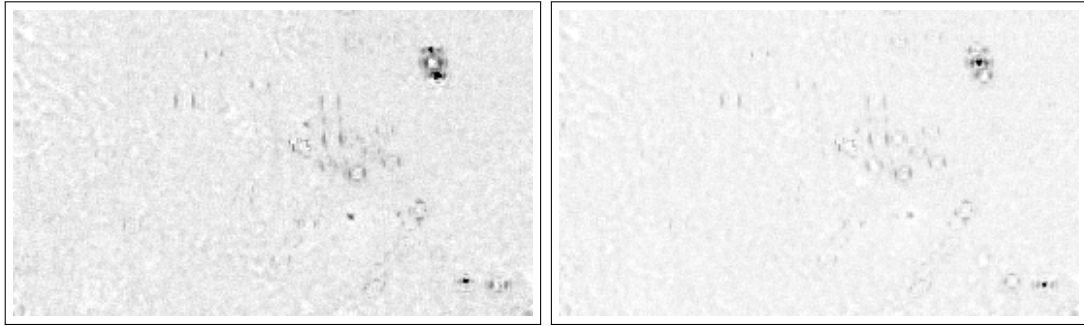
Because the residual space has smaller variance than the original space, we expect target and anomaly pixels to stand out more from the background. This has been observed for anomaly detection,^{18–20}



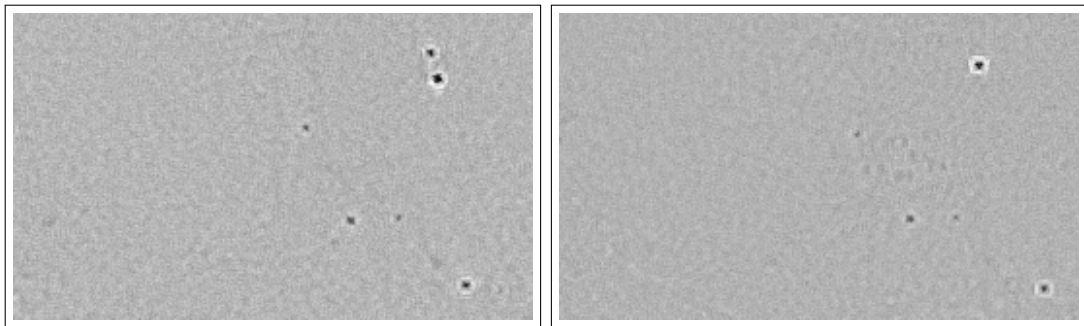
(a) Global Detection Maps



(b) Local Detection Maps



(c) Estimated fraction $\hat{\alpha}$



(d) Local Adaptive Detection Maps

Figure 5. Left maps are for blue panel targets; right maps are for red panel targets. In these experiments, in-scene target signatures were used.

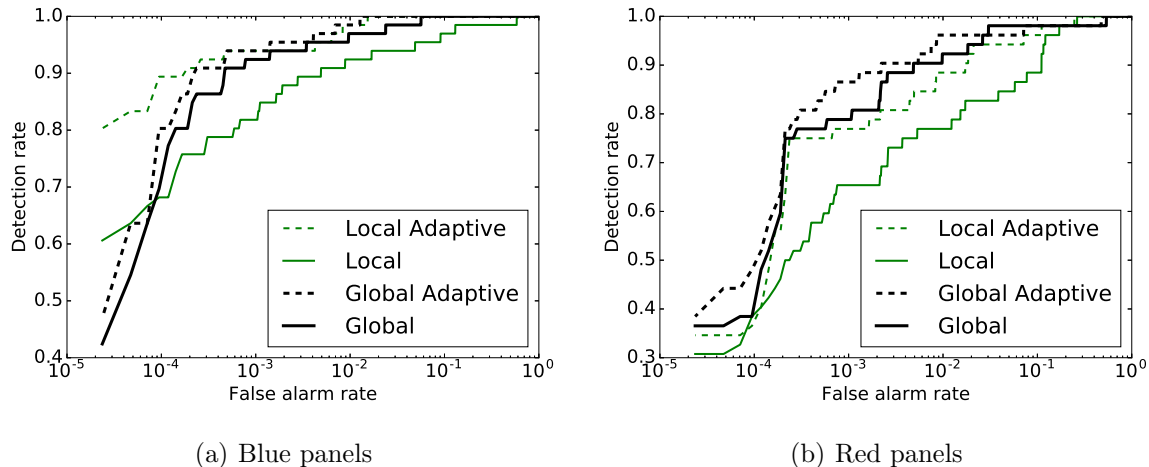


Figure 6. ROC curves compare target detection performance using locally and globally estimated backgrounds. In these experiments, in-scene target signatures were used for (a) blue panels and (b) red panels.

albeit with some glitches.²⁸ For target detection, however, this has not always been observed in practice,²¹ and the experiments presented here represent an attempt to understand and explain (and possibly fix) those negative results.

In Section 2, we showed that when the target is not additive, as for instance occurs in solid (versus gas-phase) targets, then the full residual is not necessarily desirable. In particular, when a replacement model is used, we argue for an adaptive residual; here, instead of fully “subtracting off” the best estimate of the target-free value at a pixel, a “partial” subtraction is used instead. Eq. (15) is the adaptive residual that we employ in our numerical experiments, and as Fig. 6 shows, the performance of the ACE detector improves when an adaptive instead of full residual is employed. For the blue panels, we have the result that the local background estimator leads to better performance than the global estimator, but for the red panels, the global estimator is more effective.

5. ACKNOWLEDGMENTS

The research described in this paper was supported by the U.S. Department of Energy (DOE) National Nuclear Security Administration (NNSA) Office on Nonproliferation and Verification Research and Development (DNN R&D).

REFERENCES

- [1] S. Matteoli, M. Diani, and J. Theiler, “An overview background modeling for detection of targets and anomalies in hyperspectral remotely sensed imagery,” *IEEE J. Sel. Topics in Applied Earth Observations and Remote Sensing* **7**, pp. 2317–2336, 2014.
- [2] I. S. Reed, J. D. Mallett, and L. E. Brennan, “Rapid convergence rate in adaptive arrays,” *IEEE Trans. Aerospace and Electronic Systems* **10**, pp. 853–863, 1974.
- [3] E. J. Kelly, “An adaptive detection algorithm,” *IEEE Trans. Aerospace and Electronic Systems* **22**, pp. 115–127, 1986.
- [4] F. C. Robey, D. R. Fuhrmann, E. J. Kelly, and R. Nitzberg, “A CFAR adaptive matched filter detector,” *IEEE Trans. Aerospace and Electronic Systems* **28**, pp. 208–216, 1992.
- [5] L. L. Scharf and L. T. McWhorter, “Adaptive matched subspace detectors and adaptive coherence estimators,” *Proc. 30th Asilomar Conference on Signals, Systems, and Computers*, pp. 1114–1117, 1996.

- [6] S. Kraut, L. L. Scharf, and R. W. Butler, "The Adaptive Coherence Estimator: a uniformly most-powerful-invariant adaptive detection statistic," *IEEE Trans. Signal Processing* **53**, pp. 427–438, 2005.
- [7] J. Theiler and B. R. Foy, "EC-GLRT: Detecting weak plumes in non-Gaussian hyperspectral clutter using an elliptically-contoured generalized likelihood ratio test," *Proc. IEEE International Geoscience and Remote Sensing Symposium (IGARSS)*, p. I:221, 2008.
- [8] J. W. Boardman and F. A. Kruse, "Analysis of imaging spectrometer data using-dimensional geometry and a mixture-tuned matched filtering approach," *IEEE Trans. Geoscience and Remote Sensing* **49**, pp. 4138–4152, 2011.
- [9] R. S. DiPietro, D. G. Manolakis, R. B. Lockwood, T. Cooley, and J. Jacobson, "Hyperspectral matched filter with false-alarm mitigation," *Optical Engineering* **51**, p. 016202, 2012.
- [10] A. Schaum and A. Stocker, "Spectrally selective target detection," *Proc. ISSSR (International Symposium on Spectral Sensing Research)*, p. 23, 1997.
- [11] Y. Cohen and S. R. Rotman, "Spatial-spectral filtering for the detection of point targets in multi- and hyperspectral data," *Proc. SPIE* **5806**, pp. 47–55, 2005.
- [12] C. E. Cafer, M. S. Stefanou, E. D. Nelson, A. P. Rizzuto, O. Raviv, and S. R. Rotman, "Analysis of false alarm distributions in the development and evaluation of hyperspectral point target detection algorithms," *Optical Engineering* **46**, p. 076402, 2007.
- [13] C. E. Cafer, J. Silverman, O. Orthal, D. Antonelli, Y. Sharoni, and S. R. Rotman, "Improved covariance matrices for point target detection in hyperspectral data," *Optical Engineering* **47**, p. 076402, 2008.
- [14] Y. Cohen, D. G. Blumberg, and S. R. Rotman, "Subpixel hyperspectral target detection using local spectral and spatial information," *J. Applied Remote Sensing* **6**, p. 063508, 2012.
- [15] Y. Cohen, Y. August, D. G. Blumberg, and S. R. Rotman, "Evaluating sub-pixel target detection algorithms in hyper-spectral imagery," *J. Electrical and Computer Engineering* **2012**, p. 103286, 2012.
- [16] C. C. Borel and R. F. Tuttle, "Improving the detectability of small spectral targets through spatial filtering," *Proc. SPIE* **7812**, p. 78120K, 2010.
- [17] C. C. Borel, "Methods to find sub-pixel targets in hyperspectral data," *Proc. 3rd IEEE Workshop on Hyperspectral Image and Signal Processing: Evolution in Remote Sensing (WHISPERS)*, 2011.
- [18] J. Theiler and B. Wohlberg, "Regression framework for background estimation in remote sensing imagery," *Proc. 5th IEEE Workshop on Hyperspectral Image and Signal Processing: Evolution in Remote Sensing (WHISPERS)*, 2013.
- [19] J. Theiler, "Symmetrized regression for hyperspectral background estimation," *Proc. SPIE* **9472**, p. 94721G, 2015.
- [20] J. Theiler and A. K. Ziemann, "Right spectrum in the wrong place: a framework for local hyperspectral anomaly detection," *Proc. Computational Imaging XIV*, 2016. doi:10.2352/ISSN.2470-1173.2016.19.COIMG-160.
- [21] A. K. Ziemann and J. Theiler, "Graph-based and statistical approaches for detecting spectrally variable target materials," *Proc. SPIE* **9840**, p. 98400T, 2016.
- [22] A. Schaum, "Enough with the additive target model," *Proc. SPIE* **9088**, p. 90880C, 2014.
- [23] A. Giannandrea, N. Raqueno, D. W. Messinger, J. Faulring, J. P. Kerekes, J. van Aardt, K. Canham, S. Hagstrom, E. Ontiveros, A. Gerace, J. Kaufman, K. M. Vongsy, H. Griffith, B. D. Bartlett, E. Ientilucci, J. Meola, L. Scarff, and B. Daniel, "The SHARE 2012 data campaign," *Proc. SPIE* **8743**, p. 87430F, 2013.
- [24] A. P. Schaum and B. J. Daniel, "Continuum fusion methods of spectral detection," *Optical Engineering* **51**, p. 111718, 2012.
- [25] J. Theiler, "Confusion and clairvoyance: some remarks on the composite hypothesis testing problem," *Proc. SPIE* **8390**, p. 839003, 2012.
- [26] A. Schaum, "Clairvoyant fusion: a new methodology for designing robust detection algorithms," *Proc. SPIE* **10004**, p. 100040C, 2016.
- [27] J. Theiler and B. R. Foy, "Effect of signal contamination in matched-filter detection of the signal on a cluttered background," *IEEE Geoscience and Remote Sensing Letters* **3**, pp. 98–102, 2006.
- [28] N. Hasson, S. Asulin, S. R. Rotman, and D. Blumberg, "Evaluating backgrounds for subpixel target detection: when closer isn't better," *Proc. SPIE* **9472**, p. 94720R, 2015.